

Control Interlayer Stacking and Chemical Stability of Two-Dimensional Covalent Organic Frameworks via Steric Tuning

Xiaowei Wu, Xing Han, Yuhao Liu, Yan Liu, and Yong Cui

J. Am. Chem. Soc., **Just Accepted Manuscript** • DOI: 10.1021/jacs.8b08452 • Publication Date (Web): 03 Nov 2018

Downloaded from <http://pubs.acs.org> on November 3, 2018

Just Accepted

“Just Accepted” manuscripts have been peer-reviewed and accepted for publication. They are posted online prior to technical editing, formatting for publication and author proofing. The American Chemical Society provides “Just Accepted” as a service to the research community to expedite the dissemination of scientific material as soon as possible after acceptance. “Just Accepted” manuscripts appear in full in PDF format accompanied by an HTML abstract. “Just Accepted” manuscripts have been fully peer reviewed, but should not be considered the official version of record. They are citable by the Digital Object Identifier (DOI®). “Just Accepted” is an optional service offered to authors. Therefore, the “Just Accepted” Web site may not include all articles that will be published in the journal. After a manuscript is technically edited and formatted, it will be removed from the “Just Accepted” Web site and published as an ASAP article. Note that technical editing may introduce minor changes to the manuscript text and/or graphics which could affect content, and all legal disclaimers and ethical guidelines that apply to the journal pertain. ACS cannot be held responsible for errors or consequences arising from the use of information contained in these “Just Accepted” manuscripts.

Control Interlayer Stacking and Chemical Stability of Two-Dimensional Covalent Organic Frameworks via Steric Tuning

Xiaowei Wu, Xing Han, Yuhao Liu, Yan Liu* and Yong Cui*

†School of Chemistry and Chemical Engineering and State Key Laboratory of Metal Matrix Composites, Shanghai Jiao Tong University, Shanghai 200240, China

Supporting Information

ABSTRACT: Layer stacking and chemical stability are crucial for two-dimensional covalent organic frameworks (2D COFs), but are yet challenging to gain control. In this work, we demonstrate synthetic control of both the layer stacking and chemical stability of 2D COFs by managing interlayer steric hindrance via a multivariate (MTV) approach. By co-condensation of triamines with and without alkyl substituents (ethyl and isopropyl) and a di- or trialdehyde, a family of two-, three- and four-component 2D COFs with AA, AB or ABC stacking is prepared. The alkyl groups are periodically appended on the channel walls and their contents, which can be synthetically tuned by the MTV strategy, control the stacking model and chemical stability of 2D COFs by maximizing the total crystal stacking energy and protecting hydrolytically susceptible backbones through kinetic blocking. Specifically, the COFs with higher concentration of alkyl substituents adopt AB or ABC stacking, while lower amount of functionalities leads to the AA stacking. The COFs bearing high concentration of isopropyl groups represent the first identified COFs that can retain crystallinity and porosity in boiling 20 M NaOH solution. After post-synthetic metallation with an iridium complex, the 2,2'-bipyridyl-derived COFs can heterogeneously catalyze C-H borylation of arenes, whereas the COF with isopropyl groups exhibits much higher activity than the COFs with ethyl groups and non-substituents due to the increased porosity and chemical stability. This work underscores the opportunity in using steric hindrance to tune and control layer stacking, chemical stability and properties of 2D COFs.

INTRODUCTION

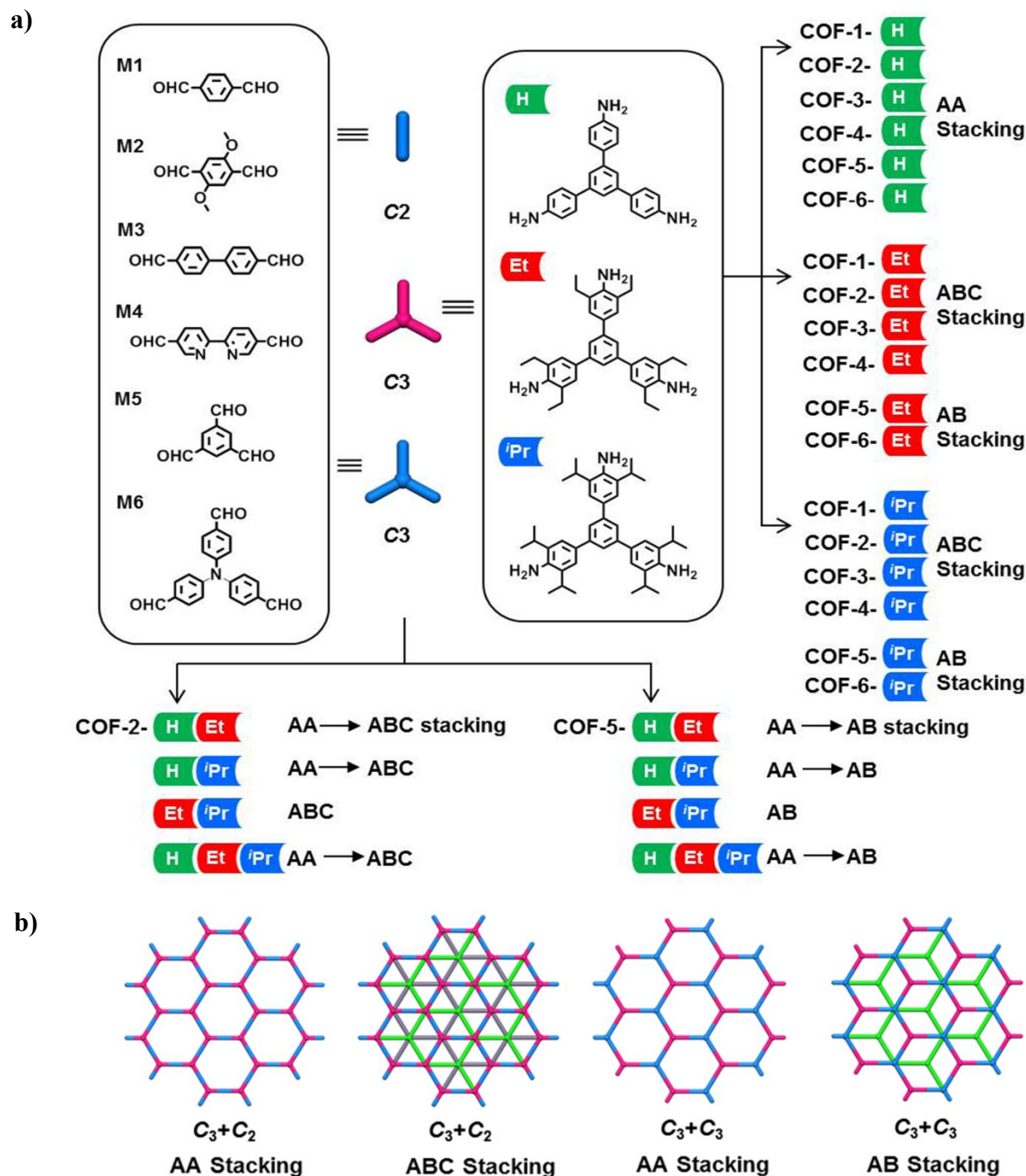
Covalent organic frameworks (COFs) are crystalline porous materials constructed by linking organic building blocks through covalent bonds.¹ Owing to their tunable compositions, structures, functions and porosity, COFs have shown potential applications in gas storage,² separation,³ catalysis,⁴ sensor,⁵ and energy storage.⁶ Among all COFs, two-dimensional (2D) COFs have received particular attentions for their unique structural and electronic properties. While the monolayers of a 2D COF can be pre-designed *via* the geometry of its building blocks, it is the stacking of monolayers into 3D structures that leads to the generation of 1D channels orthogonal to the layers, which influences interlayer electron or charge transport, thereby exerting a profound effect on their electronic and optic properties.⁷ Obviously, packing manner of the layers strongly affects not only the topology but also the physical and chemical properties of 2D COFs. Strategies have been explored to control or alter their stacking behaviors, including for example the use of propeller-shaped building units that can lock into each other to induce stacking without offset,⁸ and the utilization of donor and acceptor molecules that stack in an alternating fashion for self-complementary π -electronic interactions.^{7b,9} Nonetheless, no stacking transformation has been reported for 2D COFs to date. With few exceptions that adopt AB^{1a,10} or ABC¹¹ layer stacking, almost all reported 2D COFs exhibit eclipsed or serrated AA stacking.¹² It remains a formidable synthetic challenge to tune and control interlayer stacking of 2D COFs.

Imine-linked 2D COFs provide a convenient platform for structural control and *functional design* because of their broad monomer scope, but they are often crystallized with limited chemical stability.¹² Improved stability has been realized in systems that incorporate methoxy groups adjacent to the

aldehydes,¹³ introduce enol-keto tautomerizations that either stack regularly or offer enhanced planarity,^{1b} or convert imine linkage into amide,¹⁴ dioxin,¹⁵ oxa- and thiazole,¹⁶ and quinoline¹⁷ linkages by postsynthetic modification methods. Recent study indicated that alkylation of COFs is also capable of slowing down the rate of hydrolysis of the imine linkage.¹⁸ In this work, we report the synthetic control of both layer *stacking* (AA, AB and ABC) and chemical stability of 2D COFs by managing interlayer steric hindrance through a multivariate-component (MTV) approach.^{11c,19} A family of two-, three- and four-component 2D COFs with AA, AB or ABC stacking is prepared by co-condensation of triamines with and without two ethyl or isopropyl groups adjacent to each amine and di- or trialdehydes (Scheme 1). Mediation of different ratios of two triamines with aldehydes for COFs growth leads to the stacking transformation from ABC/AB to AA, which has never been reported for COFs before. Chemical stability of the COFs is also highly relevant to the density of incorporated alkyl groups that can protect imine linkage and hydrolytically susceptible backbones. The COFs decorated with isopropyl groups can maintain crystallinity in 20 M NaOH solution at r.t. and 100 °C for one week, topping any reported stable COFs against harsh base condition. When metallated with [Ir(COD)(OMe)₂], the 2,2'-bipyridine-derived COF containing isopropyl groups can be an efficient active and recyclable heterogeneous catalyst for arene C-H borylation, whereas the COFs containing ethyl groups and non-substituents give much low activities. The addition of bulky alkyl substituents to COFs leads to greatly enhanced catalytic activity by increasing porosity and chemical stability.

RESULTS AND DISCUSSION

Synthesis and Characterization. The 2D COFs **1-6-H** have been reported previously and adopts a AA stacking mode^{13,20}. As

Scheme 1. (a) Construction of the binary, ternary and quaternary COFs and (b) their stacking modes

shown in Scheme 1, COFs 1-6-*i*Pr and 1-6-Et were synthesized by reacting triamine *i*Pr²¹ (60 mg, 0.1 mmol) or Et (52 mg, 0.1 mmol) with di- or tri-aldehyde (0.15 mmol or 0.1 mmol) in EtOH in the presence of acetic acid (9 M, 0.2 mL) at 120 °C for three days, which afforded yellow crystalline solids in 74-95% yields (Scheme 1). All COFs are stable in common organic solvents.

In the FT-IR spectra of the series of Et- and *i*Pr-COFs, the characteristic C=O stretching bands (~1689 cm⁻¹) almost disappeared, indicative of the consumption of the aldehydes (Figure S1). Strong stretching vibration bands attributed to the new generation of C=N linkages were observed at ~1631 cm⁻¹. In

the ¹³C CP-MAS NMR spectra, isopropyl group signals appeared at 23 and 31 ppm, ethyl group signals appeared at 14 and 25 ppm and the characteristic signals due to C=N bonds were observed at 162 ppm (Figure S2). The aldehyde carbon peaks were barely present. The chemical shifts of other fragments are consistent with those of the monomers. Thermal gravimetric analysis revealed that those COFs exhibited no weight loss under N₂ on heating to 380 °C (Figure S3). Transmission electron microscopy (TEM) images of the COFs reveal that the materials crystallize in the form of platelets with very large domain sizes of 100-300 nm, indicative of the 2D nature of these structures (Figure S5).

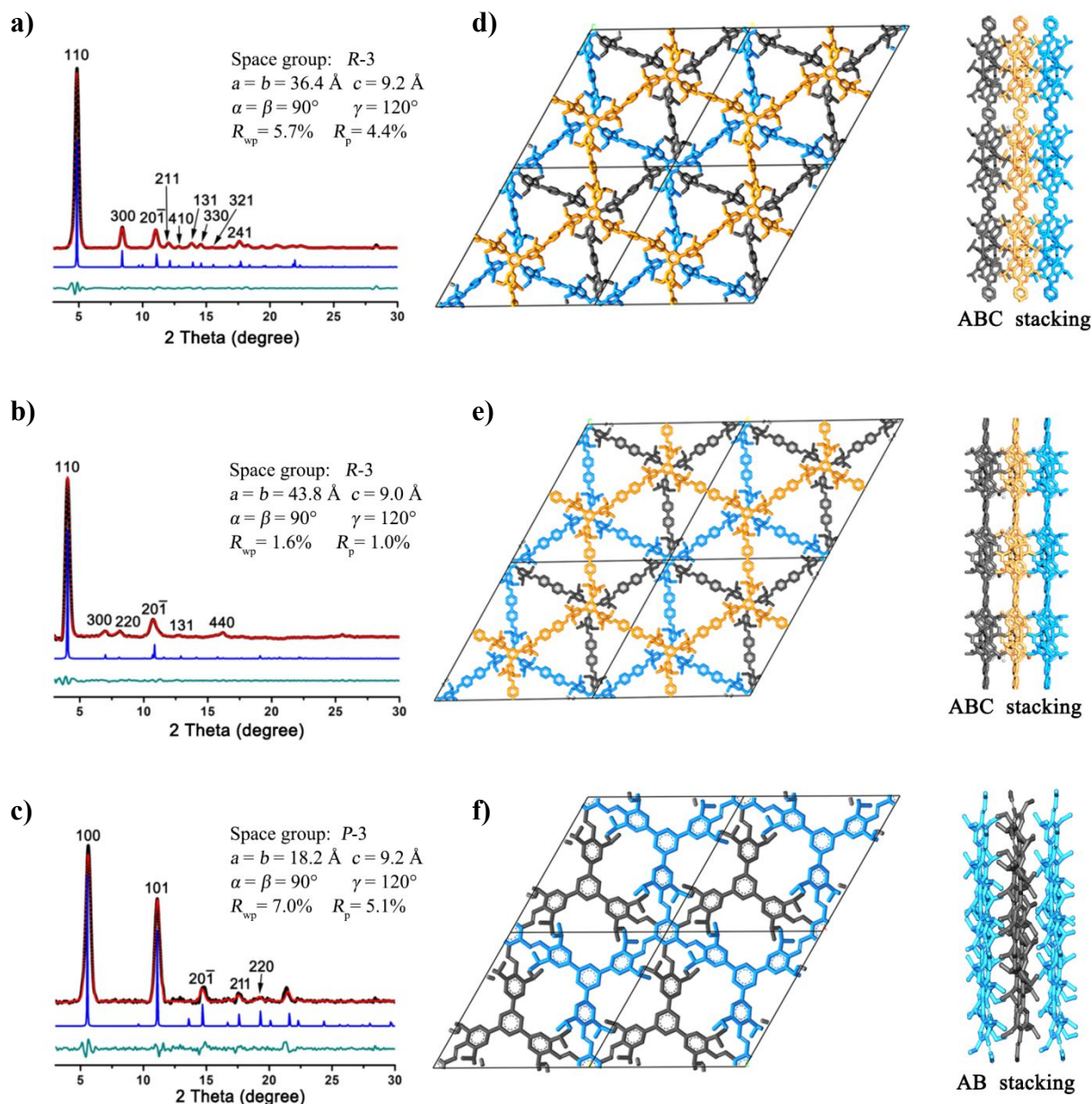


Figure 1. PXRD patterns of COFs (a) **1-Pr** (b) **4-Pr** and (c) **5-Pr** with the experimental profiles in black, Pawley-refined profiles in red, calculated profiles in blue, and the differences between the experimental and refined PXRD patterns in dark cyan. Top (left) and side (right) views of the corresponding refined 2D crystal structures of (d) **1-Pr** (e) **4-Pr** and (f) **5-Pr**.

Crystal Structure. The crystalline structures of the COFs were determined by powder X-ray diffraction (PXRD) analysis with Cu $K\alpha$ radiation. As revealed from PXRD analyses, COFs **1-Pr** and **2-Pr** show high crystallinity, exhibiting the first intense peak at a low angle 4.9° (2θ), which corresponds to the (110) reflection plane, along with minor peaks at 8.4° , 11.4° , 12.5° , 14.5° , and 17.8° , attributed to the (300), ($20\bar{1}$), (211), (131) and (241) reflection planes, respectively (Figures 1a, S14). For **3-Pr** and **4-Pr**, the first and most intense peak corresponding to the (110) reflection plane appears at $\sim 4^\circ$, with other minor peaks at 7.0° , 8.0° , 10.7° , 12.9° and 16.1° attributed to the (300), (220), ($20\bar{1}$), (131), and (440) reflection planes, respectively (Figures 1b, S14). COF **5-Pr** gave strong PXRD peaks at 5.5° , 11.1° , 14.7° , 17.6° ,

and 19.3° , corresponding to the (100), (101), ($20\bar{1}$), (211) and (220) reflection planes, respectively (Figure 1c), and **6-Pr** gave strong PXRD peaks at 4.8° , 8.4° , 9.7° , 10.9° , 11.9° , 12.8° and 13.8° , corresponding to the (100), (110), (200), (001), (101), (120) and (111) reflection planes, respectively (Figure S14).

In order to elucidate the structures of the COFs and calculate the unit cell parameters, three types of possible 2D structures were generated for each of them, that is, eclipsed stacking (AA), staggered stacking (AB and ABC) models were built and optimized by the Materials Studio Forcite molecular dynamics module method (Figure S15). It is found that the total crystal stacking energy of ABC stacking ($116.52 \text{ kcal mol}^{-1}$) for COF **1-Pr** is much higher

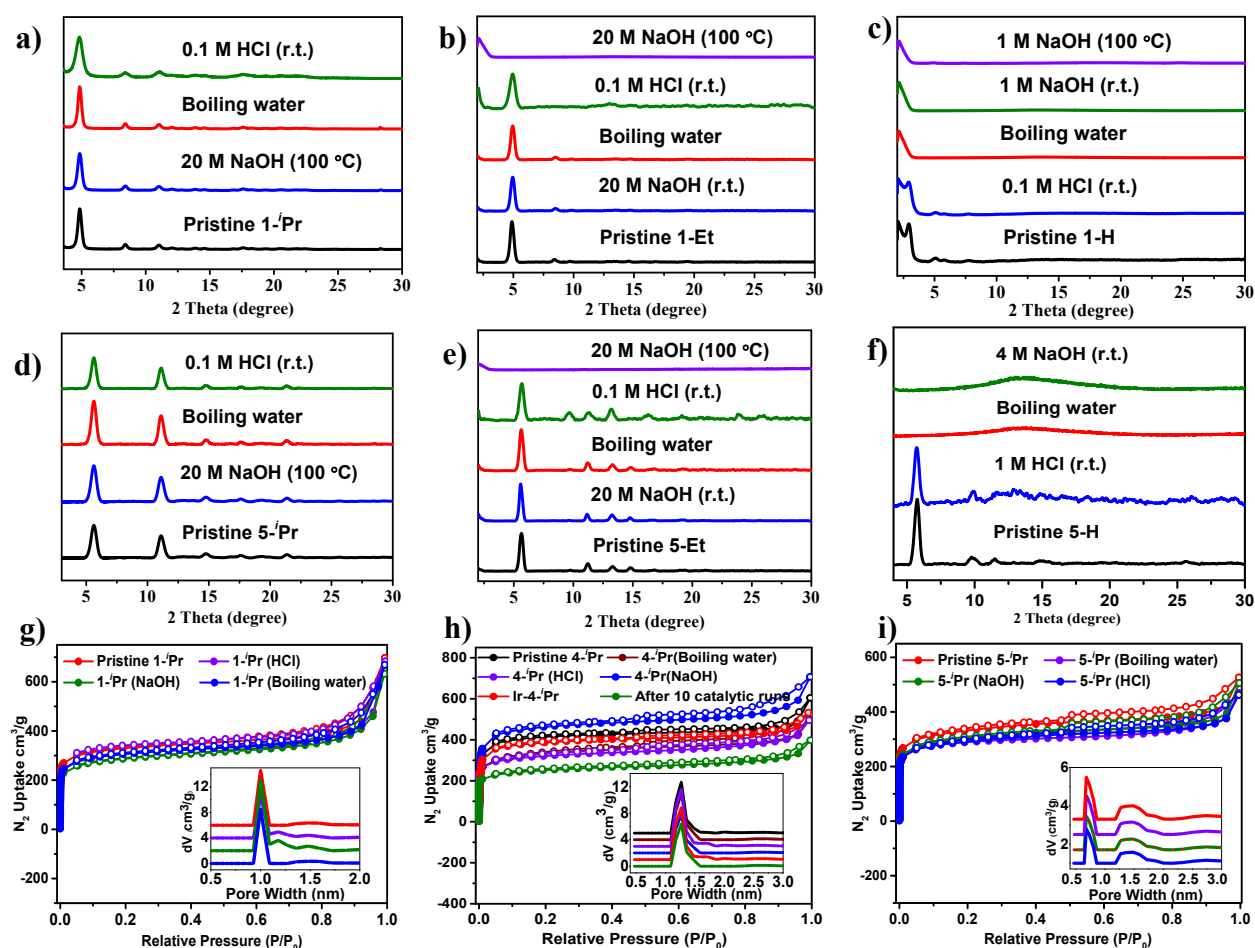


Figure 2. PXRD patterns of COFs (a) **1-*i*-Pr** (b) **1-Et** (c) **1-H** (d) **5-*i*-Pr** (e) **5-Et** (f) **5-H** upon treatment in different solvents for 7 days. N₂ adsorption-desorption isotherms (77 K) and pore size distribution profiles (insert) of the COFs (g) **1-*i*-Pr** (h) **4-*i*-Pr** (i) **5-*i*-Pr** after treatment in boiling water, 0.1 M HCl and 20 M NaOH solutions at 100 °C for 7 days.

than those of the AA (44.67 kcal·mol⁻¹) and AB (70.33 kcal·mol⁻¹) stacking, and the total crystal stacking energy of AB stacking for COF **5-*i*-Pr** (119.40 kcal·mol⁻¹) is much higher than those of AA (37.51 kcal·mol⁻¹) and ABC (73.21 kcal·mol⁻¹) stacking. Similar behaviors were found in COFs **2-4-*i*-Pr** and **6-*i*-Pr** (Table S4). The experimental PXRD patterns for **1-4-*i*-Pr** match well with the simulated patterns of the staggered stacking (ABC) model in the trigonal *R*-3 space group (Figure 1). However, the models proposed for PXRD patterns of **5-** and **6-*i*-Pr** agreed well with the simulated pattern generated from the staggered stacking (AB) of the 2D layers in the trigonal *P*-3 space group (Figures 1c and S14). Pawley refinements gave optimized parameters ($a = b = 36.40$ Å and $c = 9.21$ Å for **1-*i*-Pr**; $a = b = 36.23$ Å and $c = 9.05$ Å for **2-*i*-Pr**; $a = b = 44.03$ Å and $c = 9.03$ Å for **3-*i*-Pr**; $a = b = 43.80$ Å and $c = 9.04$ Å for **4-*i*-Pr**), which provided good agreement factors ($R_p = 4.48\%$ and $R_{wp} = 5.76\%$ for **1-*i*-Pr**; $R_p = 3.57\%$ and $R_{wp} = 5.54\%$ for **2-*i*-Pr**; $R_p = 2.39\%$ and $R_{wp} = 3.73\%$ for **3-*i*-Pr**; $R_p = 1.03\%$ and $R_{wp} = 1.60\%$ for **4-*i*-Pr**). Similarly, unit cell parameters were obtained for **5-*i*-Pr** ($a = b = 18.39$ Å, $c = 9.19$ Å) and **6-*i*-Pr** ($a = b = 21.09$ Å, $c = 8.03$ Å), with acceptably low residuals ($R_p = 5.07\%$ and $R_{wp} = 7.04\%$ for **5-*i*-Pr**; $R_p = 4.12\%$ and $R_{wp} = 5.66\%$ for **6-*i*-Pr**). COFs **1-4-Et** showed the isomorphous structures to **1-*i*-Pr** while **5-** and **6-Et** preferred AB stacking (Figures S14 and S15).

The porosity of these COFs was examined by measuring N₂ sorption isotherms at 77 K on the activated samples. The adsorption curves of them exhibited type-I isotherm (Figures 2 and S11), a characteristic of microporous materials. The Brunauer-Emmett-Teller (BET) surface areas of them range from 355 to 1197 m²·g⁻¹ (Table 1). The nonlocal density functional theory (NLDFT) gave rise to a narrow pore size distribution for COFs **1-6-*i*-Pr/Et**, respectively, in good agreement with the simulated values (Table 1 and Figures 2 and S11).

Chemical Stability. The chemical stability of the COFs was examined by PXRD and N₂ sorption isotherms after 7 days treatment in boiling water, 0.1 M HCl at r.t and 20 M NaOH (r.t or 100 °C). All binary COFs are stable in boiling water, as evidenced by the almost unchanged PXRD patterns (Figures 2 and S6), BET surface areas (Figure 2 and Table 1) and residue weight percentage (Figure S13). In 0.1 M HCl solution, all these COFs retained their original structures, but gave a slightly decreased crystallinity. A small decrease in signal-to-noise ratio and a slight to moderate decrease in the surface area of them indicate just partial structural collapse upon treatment (Table 1). Remarkably, all *i*-Pr-COFs were stable in 20 M NaOH solution at 100 °C and retained good crystallinity. The as-treated samples showed BET surface areas close to or higher than the pristine samples. The

increase in surface areas of **2-4-*i*Pr** and **6-*i*Pr** may be attributed to the degradation of oligomers trapped in the networks in strong alkaline solutions, which were not easy to be removed by common solvent washing or vacuum pump activation. Therefore, the *i*Pr-COFs show the ultra-strong alkali-resistance ability and the modest level of acid-resistance. This is consistent with that protons have a smaller radius than hydroxyl ions (2.8 vs 3.0 Å) and can easily attack and decompose dynamic C=N bonds.

Table 1. BET surface areas of the COFs^a

COF	BET surface areas (m ² /g)				Pore width (nm)
	Pristine	H ₂ O (100 °C)	HCl (0.1 M)	NaOH ^b (20 M)	
1-<i>i</i>Pr	970	960	906	967	1.00
2-<i>i</i>Pr	1000	942	956	1061	0.82
3-<i>i</i>Pr	718	700	594	835	1.29
4-<i>i</i>Pr	1197	1055	1130	1437	1.26
5-<i>i</i>Pr	1068	976	863	997	0.72
6-<i>i</i>Pr	824	797	786	940	0.81
1-Et	768	752	277	792	0.93
2-Et	755	755	119	722	0.81
3-Et	355	342	133	296	1.15
4-Et	494	423	221	481	1.17
5-Et	567	513	443	560	0.69
6-Et	688	649	344	702	0.68

^aAfter treatment under different conditions for 7 days. ^bTreated at 100 °C for **1-6-*i*Pr** and at r.t. for **1-6-Et**.

Compared with COFs **1-6-*i*Pr**, **1-6-Et** gave decreased chemical stability and porosity. For example, both **1-** and **5-Et** are stable in boiling water and 0.1 M HCl at r.t., but lost crystallinity when the treated temperature was increased from r.t. to 100 °C (Figures 2b, 2e and S7). In sharp contrast, the analogous COFs containing no alkyl groups gave low chemical stability. For example, COF **1-H** was stable in 0.1 M HCl at r.t., but after soaking in boiling water and 1 M NaOH solution, the sample was partly dissolved and got amorphous (Figure 2c). In COFs **1-6-*i*Pr/Et**, the bulky isopropyl and ethyl groups were positioned near nitrogen atoms that can protect C=N bonds and hydrolytically susceptible backbones through kinetic blocking, leading to higher chemical stability than the nonalkylated **1-6-H**. However, the substituted ethyl groups were not so hydrophobic and bulky as that of the isopropyl groups to protect the susceptible backbones, and so COFs **1-6-Et** gave slightly lower chemical stability than **1-6-*i*Pr**. As far as we know, with structural ultrastability in basic solutions up to 20 M NaOH solution at 100 °C for 7 days, COFs **1-6-*i*Pr** not only top the list of COFs, but also surpass all reported MOFs²² and molecular sieves (ZSM-5,²³ MCM-41,²³ SBA-15²⁴ etc) regarding alkali resistance.

Among hundreds of 2D COFs that have been constructed, only a handful of them adopt AB or ABC stacking.^{10,11} Influences of substitutes on stacking modes have been reported in a 2D COF, in which methyl groups extending out-of-plane of layers and the inclined stacking mode was obtained.^{7a} In this work, when the bulky alkyl substituents are attached to the COFs, both AB and ABC stacking models are more steric favorable than AA stacking, thus to avoid the close repulsion between adjacent layers. As shown in Scheme 1, we hypothesized that ABC stacking is favorable for the combination of C₂- and C₃-symmetric monomers,

and AB stacking is favorable for the combination of C₃- and C₃-symmetric monomers. Take a deep look inside the molecular arrangement in each *i*Pr unit, the two central aromatic cores of adjacent layers overlapped in a manner that one *i*Pr core rotated 60° around the c-axis (Figure 3). Each of the three isopropyl-arms in *i*Pr rotated around the central core about 45°, allowing for enough space between the bulky groups while maintaining a close-packed orientation of the backbone. Similar behaviors were observed for the Et-based COF. Confirming our hypothesis, the steric effect of the building blocks defines the position of each building unit within adjacent COF layers, which guides the attachment of successive layers in a AB or ABC stacking manner.⁸

For the C₃ + C₃ combination, the AB stacking enables the adjacent layers to be precisely arranged to fulfill the π-π interactions, whereas no π-π interactions are involved in the ABC stacking. Crystal stacking energy for different stacking modes was calculated to further validate the stacking preference. The calculated total crystal stacking energy for the AB stacked **5-*i*Pr** (119.40 kcal/mol) is higher than that of the possible ABC and AA ones (73.21 and 37.51 kcal/mol, respectively), supporting the observed AB stacking in **5-*i*Pr**. For the C₂ + C₃ combination, although π-π interactions exist in both AB and ABC stacking, the density of phenyl pairs with π-π interactions for ABC stacking is calculated to be 2.84 times higher than that of AB stacking (Figure S22), in agreement with the stacking mode of **1-*i*Pr**. Table S4 showed that the calculated total crystal stacking energy for the ABC stacked **1-*i*Pr** (116.52 kcal/mol) is higher than those of the possible AB and AA ones (70.33 and 44.67 kcal/mol, respectively), supporting that ABC stacking instead of AA and AB was adopted by **1-*i*Pr**.

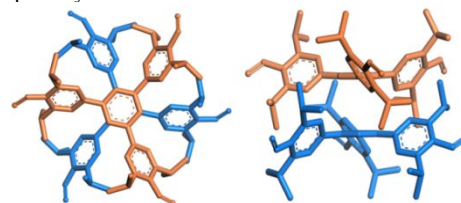


Figure 3. Top (left) and side (right) views of the overlapping the *i*Pr cores between adjacent layers in COF **2-*i*Pr**.

Tuning of Layer Stacking and Chemical Stability. Although the nonalkylated COFs **1-6-H** adopted AA stacking,²⁰ their analogues alkylated **1-4-*i*Pr/-Et** adopted ABC stacking and **5-** and **6-*i*Pr/-Et** adopted AB stacking. To further study the influence of alkyl substituents on layer stacking, three series of ternary COFs **2-H_{1-x}-*i*Pr_x-Et_x** and **2-Et_{1-x}-*i*Pr_x** containing different molar ratios of two triamine monomers were prepared (Scheme 1). Remarkably, PXRD patterns of **2-H_{1-x}-*i*Pr_x** are changed with molar ratios of *i*Pr to H. When x>8/9, the diffraction peaks were found at 4.9°, 8.5°, 11.4°, 12.5°, 14.5°, and 17.8°, attributed to the (110), (300), (20 $\bar{1}$), (211), (131) and (241) reflection planes, respectively, indicating the generation of the ABC stacked product inherited from **2-*i*Pr** (Figures 4a and 4e). However, when 1/9<x<8/9, two sets of diffraction peaks due to a mixture of AA and ABC stacked COFs were detected. For example, in **2-H_{1/2}-*i*Pr_{1/2}** (Figure 4e), one set of peaks due to the ABC stacked product was observed at 4.9°, 8.5°, 11.4°, assigned to the (110), (300), (20 $\bar{1}$) facets, respectively. Another set of peaks due to the AA stacked product was seen at 2.9°, 4.8°, 5.8°, 7.6° and 9.86°, assigned to the (100), (110), (200), (210) and (220) facets, respectively. When 0<x<1/9, only one set of peaks due to the AA stacking product was observed at 2.9°, 4.8°, 5.8°, 7.6° and 9.86°,

assigned to the (100), (110), (200), (210) and (220) facets (Figures 4a and 4e).

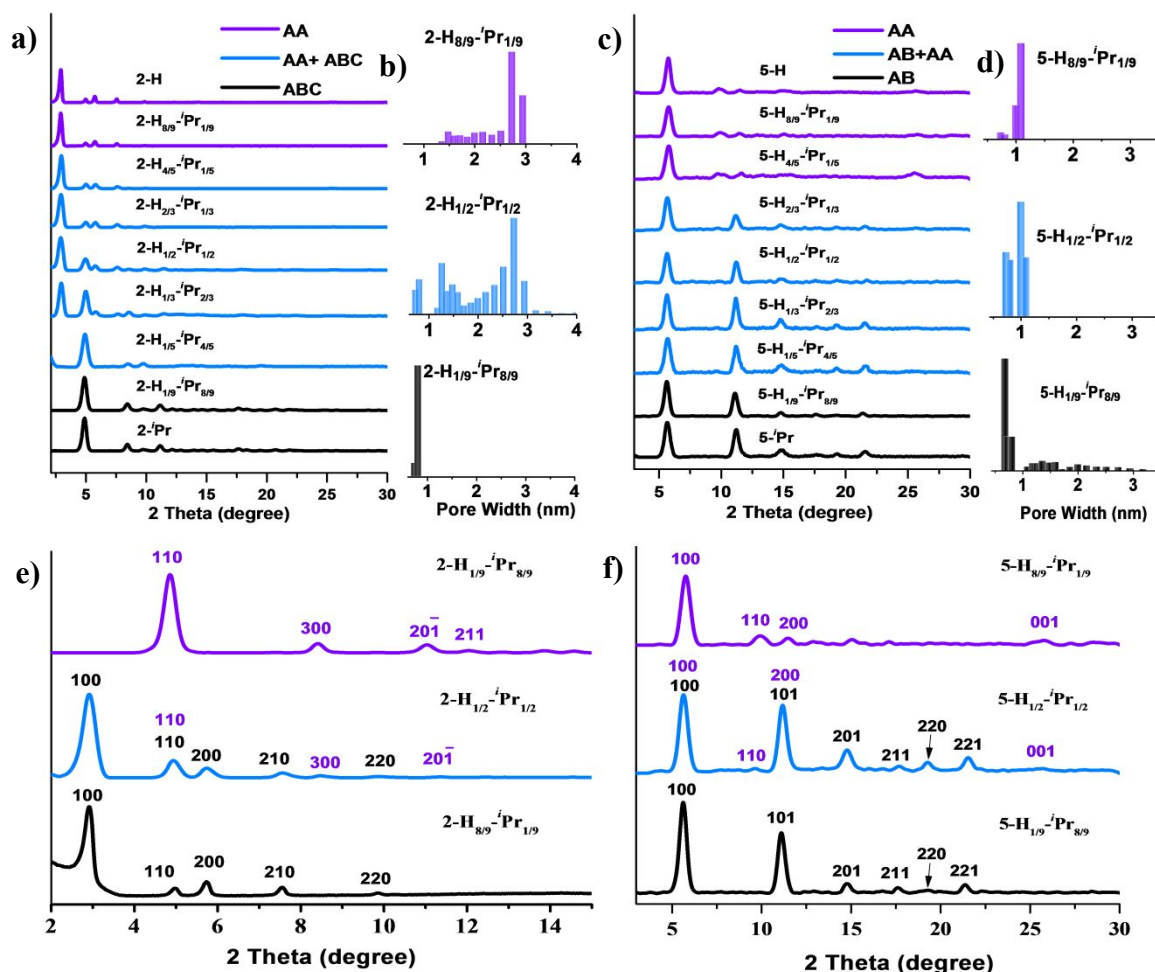


Figure 4. PXRD patterns and pore size distributions showing the stacking transformation from AA to ABC/AB stacking in the MTV COFs. (a) PXRD patterns for $2\text{-H}_{1-x}\text{-}^i\text{Pr}_x$ and (c) $5\text{-H}_{1-x}\text{-}^i\text{Pr}_x$. Pore size distribution of COFs (b) $2\text{-H}_{1-x}\text{-}^i\text{Pr}_x$ and (d) $5\text{-H}_{1-x}\text{-}^i\text{Pr}_x$. PXRD peaks indexing for (e) COFs $2\text{-H}_x\text{-}^i\text{Pr}_{1-x}$ and (f) $5\text{-H}_x\text{-}^i\text{Pr}_{1-x}$.

COFs $2\text{-H}_{1-x}\text{-Et}_x$ revealed a similar tendency (Figure S7). For $x > 1/2$ and $0 < x < 1/9$, ABC and AA stacking of the layers were adopted, respectively, and for $1/9 < x < 1/2$, both AA and ABC stacking of the layers were obtained individually. Pore size distributions calculated from N_2 sorption isotherms were consistent with the results of PXRD (Figure 4b), SEM (Figure S40-4r) and ^1H NMR (Figure S10) obtained from digested $2\text{-H}_{1-x}\text{-}^i\text{Pr}_x/\text{Et}_x$ confirmed that both ^iPr (or Et) and H existed in the products. In contrast, all three COFs $2\text{-Et}_{1/9}\text{-}^i\text{Pr}_{8/9}$, $2\text{-Et}_{1/2}\text{-}^i\text{Pr}_{1/2}$ and $2\text{-Et}_{8/9}\text{-}^i\text{Pr}_{1/9}$ exhibited almost the same PXRD patterns as those of $2\text{-}^i\text{Pr}$ and 2-Et , indicating the formation of the ABC stacked products (Figure S8). Therefore, through mediation of different ratios of ^iPr (or Et) to H with M2 , the resulting $2\text{-H}_{1-x}\text{-}^i\text{Pr}_x\text{-Et}_x$ can evolve to different stacking manners, from ABC, via a transitional period of mixtures of ABC and AA, to the single AA stacking. To the best of our knowledge, this is the first report on the stacking mode transformation in 2D COFs.¹⁰⁻¹²

Previous studies showed that, if suitable substituents are introduced into the skeleton of 2D COFs, steric repulsion between the substituents of layers will affect the COF structures.^{7a,25} That

means the path to one stacking manner may be blocked, and only other stacking models that can significantly alleviate steric repulsion can be generated. In the case of $2\text{-H}_{1-x}\text{-}^i\text{Pr}_x/\text{Et}_x$, the portion of ^iPr (or Et) mainly determine the level of steric repulsion between layers. In the high level of steric repulsion ($8/9 < x < 1$ and $1/2 < x < 1$, respectively), the COFs adopted the ABC staking mode inherited from $2\text{-}^i\text{Pr}_x$ and 2-Et , since the locking and docking sites generated from ABC stacking greatly release the repulsion. In the low degree of steric repulsion ($0 < x < 1/9$ for both cases), they preferred to AA stacking inherited from 2-H , which can generate big mesopores and provided enough space for the low density of alkyl groups to rotate flexibly to alleviate steric repulsion. In the moderate level of repulsion ($1/9 < x < 8/9$ for $2\text{-H}_{1-x}\text{-}^i\text{Pr}_x$, $1/9 < x < 1/2$ for $2\text{-H}_{1-x}\text{-Et}_x$), the route to generate the single AA or ABC stacked products was prohibited, because considerable steric repulsion still existed to prevent the formation of eclipsed AA stacking of layers. Staggered ABC stacking was also excluded, due to the fact that, to build well-defined periodic docking sites, more ^iPr (or Et) groups were needed to maintain a close-packed orientation of the periodic and intact backbone. As a result, two COFs with AA and ABC stacking were obtained

individually. The SEM images of $2\text{-H}_{1-x}\text{-}^i\text{Pr}_x$ (Figures S40-4r) are informative towards the phase purity, further confirming the pure

phases AA ($0 < x < 1/9$) and ABC ($8/9 < x < 1$), or the existence of two separated phases of AA and ABC ($1/9 < x < 8/9$).

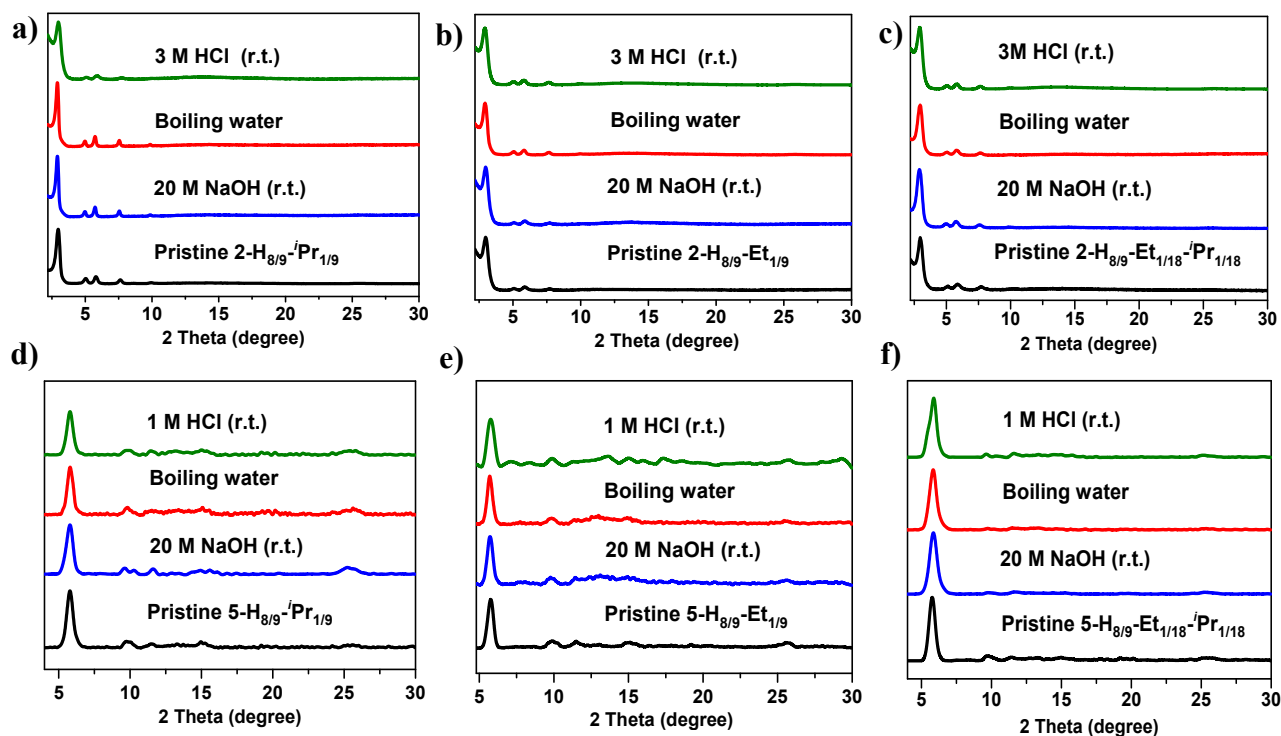


Figure 5. PXRD patterns the MTV-COFs (a) $2\text{-H}_{8/9}\text{-}^i\text{Pr}_{1/9}$ (b) $2\text{-H}_{8/9}\text{-Et}_{1/9}$ (c) $2\text{-H}_{8/9}\text{-Et}_{1/18}\text{-}^i\text{Pr}_{1/18}$ (d) $5\text{-H}_{8/9}\text{-}^i\text{Pr}_{1/9}$ (e) $5\text{-H}_{8/9}\text{-Et}_{1/9}$ and (f) $5\text{-H}_{8/9}\text{-Et}_{1/18}\text{-}^i\text{Pr}_{1/18}$ upon treatment in different solvents for 7 days.

To further study the influences of steric effects on the 2D structure, we prepared ternary COFs $5\text{-H}_{1-x}\text{-}^i\text{Pr}_x\text{-Et}_x$ and $5\text{-Et}_{1-x}\text{-}^i\text{Pr}_x$ by varying the molar ratios of different triamine monomers undersolvothermal reaction conditions (Scheme 1). PXRD showed that, the ternary layer structures adopted AA and AB stacking for $0 < x < 1/5$ and $x > 4/5$, respectively, and a mixture of AA and AB stacking for $1/5 < x < 4/5$ (Figures 4c, 4d, 4f and S7), whereas, as expected, all COFs $5\text{-Et}_{1-x}\text{-}^i\text{Pr}_x$ (Figure S8) adopted only AB stacking. Also, we prepared quaternary COFs 2- and $5\text{-H}_{1-x-y}\text{-Et}_x\text{-}^i\text{Pr}_y$. Depending on the ratios of different monomers, the MTV COFs $2\text{-H}_{1-x-y}\text{-Et}_x\text{-}^i\text{Pr}_y$ can adopt AA, ABC or a mixture of AA and ABC stacking, and $5\text{-H}_{1-x-y}\text{-Et}_x\text{-}^i\text{Pr}_y$ adopt AA, AB or a mixture of AA and AB stacking (Figure S8). Taken together, the above findings indicated the stacking modes of the 2D COFs are determined by the interlayer repulsion and can be controlled by carefully tuning the concentration of steric monomers.

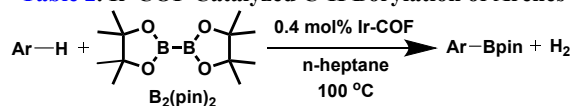
The chemical stability of the MTV COFs was also tested in acid, base and boiling water by PXRD and N_2 sorption isotherms. As shown in Figure 5, both ternary COFs $2\text{-H}_{8/9}\text{-}^i\text{Pr}_{1/9}\text{-Et}_{1/9}$ and quaternary COFs $2\text{-H}_{8/9}\text{-Et}_{1/18}\text{-}^i\text{Pr}_{1/18}$ can retain their crystallinity and porosity in boiling water, 20 M NaOH solution at r.t and 3 M HCl solution at r.t (Figures 5a, 5b and 5c), which is about 30 times in resistance against HCl solution than that of COFs $2\text{-}^i\text{Pr}/\text{Et}$. The improved acid stability may be due to the introduction of H monomers, which induce the layer stacking from ABC to AA to strengthen the interlayer interactions. However, the acid stability is lower than that of COF 2-H (stable in 12 M HCl), probably as a consequence of steric interactions between the bulky pendent isopropyl/ethyl and methoxyl groups that decrease interlayered

interactions. In addition, COFs $2\text{-H}_{1/9}\text{-}^i\text{Pr}_{8/9}\text{-Et}_{8/9}$ and $2\text{-H}_{1/9}\text{-Et}_{4/9}\text{-}^i\text{Pr}_{4/9}$ gave similar chemical stability to the binary COF- $2\text{-}^i\text{Pr}/\text{Et}$ (Figure S9). Meanwhile, both COFs $5\text{-H}_{8/9}\text{-}^i\text{Pr}_{1/9}\text{-Et}_{1/9}$ and $5\text{-H}_{8/9}\text{-Et}_{1/18}\text{-}^i\text{Pr}_{1/18}$ exhibiting comparable chemical stability to 5-Et , but much improved water and base stability compared with 5-H (Figures 5d, 5e, 5f). For example, these MTV COFs retained high crystallinity and porosity in boiling water and 20 M NaOH solution at r.t., whereas the binary COF 5-H became amorphous quickly in boiling water and 4 M NaOH solution (Figure 2f). This enhanced stability may be ascribed to the fact that the bulky isopropyl or ethyl groups in the MTV COFs can protect hydrolytically susceptible imine bonds through kinetic blocking. It is likely that the MTV strategy can be used not only to guide the stacking mode of 2D COFs, but also to control the chemical stability, which was determined by the nature of the main component of building blocks.

Heterogeneous Catalysis. We have employed COFs $4\text{-}^i\text{Pr}/\text{Et}/\text{H}$ for heterogeneous catalysis by taking advantage of their 2, 2'-bipyridine open sites. 2,2'-bipyridine and its derivatives have been widely used as chelating ligands for forming metal complexes in coordination chemistry.²⁶ For example, Iridium-bipyridine complexes are highly active catalysts for many meaningful reactions including C-H borylation of arenes and heteroarenes.²⁷ However, such homogeneous catalysts have very open coordination environments and are prone to deactivation *via* intermolecular pathways. Therefore, to inhibit deactivation pathways, Ir-bipyridine complexes have been immobilized on diverse porous solid supports such as silica²⁸ and metal-organic frameworks (MOFs).²⁹

Metalation of a microcrystalline powder of **4-*i*Pr-Et-H** with [Ir(COD)(OMe)₂] in THF at r.t affording light brown powders as **Ir-4-*i*Pr-Et-H**. Inductively coupled plasma optical emission spectrometry (ICP-OES) analyses revealed that the Ir loadings were 4.1 wt % for **Ir-4-*i*Pr**, 6.5 wt % for **Ir-4-Et**, and 4.9 wt % for **Ir-4-H**, which are consistent with Ir coordination to 13.24, 19.83, and 11.36% of the total bipyridine sites, respectively. This indicates that only part of pores in the frameworks is occupied by Ir, ensuring the open channels for catalysis. After optimization of reaction conditions, **Ir-4-*i*Pr** was found to be an active catalyst for dehydrogenative borylation of aromatic C-H bonds using B₂(pin)₂ (pin = pinacolate) as the borylating agent to provide aryl boronates, which are versatile reagents in organic synthesis.²⁸ As shown in Table 2, in the presence of 0.4 mol% **Ir-4-*i*Pr**, benzene and thiophene were borylated to give products in 100 % yield at 100 °C for 24 h (Table 2, entries 1 and 14). Pure borylated products can be readily obtained by removing the solid catalyst *via* centrifugation followed by removal of the volatiles. Halogen and alkoxy functional groups were well tolerated under the reaction conditions (Table 2, entries 5, 9, 13). The borylation occurred at the least sterically hindered C-H bonds of arenes (Table 2, entries 5, 9, 13) and tended to activate 2-position of C-H bonds in heteroarenes (Table 2, entries 15 and 16).

Table 2. Ir-COF Catalyzed C-H Borylation of Arenes^a



entry	product	catalyst	time (h)	yield (%) ^b
1		Ir-4-<i>i</i>Pr	24	100 (51) ^c
2		Ir-4-Et	24	85 (48) ^c
3		Ir-4-H	24	76
4		Ir-bipy	48	61 ^d
5		Ir-4-<i>i</i>Pr	24	100 (76) ^c
6		Ir-4-Et	24	88 (74) ^c
7		Ir-4-H	24	81
8		Ir-bipy	24	80 ^d
9		Ir-4-<i>i</i>Pr	24	100
10		Ir-4-Et	24	84
11		Ir-4-H	24	79
12		Ir-bipy	24	63 ^d
13		Ir-4-<i>i</i>Pr	24	100
14		Ir-4-<i>i</i>Pr	24	100
15		Ir-4-<i>i</i>Pr	24	100 o:m = 92:8
16		Ir-4-<i>i</i>Pr	24	95 o:m = 90:10

^aReaction conditions: 0.4 mol % Ir loading, 0.52 mmol B₂(pin)₂, 1.0 mmol of arene, 2.0 mL of n-heptane, 100 °C, reflux under N₂. For entries 1-4, 14 and 15, neat arene was used. ^bCalculated by ¹H NMR. ^cCatalyzed by 0.4 mol% the amorphous COF. ^dCatalyzed by 0.4 mol% Ir(bipy)(COD)(OMe) as the homogeneous control.

Compared with **Ir-4-*i*Pr**, **Ir-4-Et-H** displayed obviously decreased catalytic activities in borylation of arenes. For example, under otherwise identical conditions, borylation of benzene, 3-(trifluoromethyl)anisole and 1,3-dichlorobenzene catalyzed by **Ir-4-Et** afforded 85%, 88% and 84% yields of the products,

respectively, and catalyzed by **Ir-4-H** produced 76%, 81% and 79% yields. All yields are much lower than those obtained with **Ir-4-*i*Pr**, as shown in Table 2 (entries 2, 3, 6, 7, 10 and 11). Therefore, the above results showed that the catalytic activities of the three COFs are in the order **Ir-4-*i*Pr** > **Ir-4-Et** > **Ir-4-H**. This trend could be explained in the following two reasons. Firstly, compared with the eclipsed stacked **Ir-4-H**, the ABC packing of **Ir-4-Et/Pr** has divided the large hexagonal open channels into smaller triangular micropores with more suitable pore widths. Indeed, higher surface areas were recorded for **Ir-4-Et/Pr** (336 and 1084 m²/g, respectively) compared with **Ir-4-H** (217 m²/g). The transformation of pore shapes via steric tuning may expose more readily accessible active sites for reactants and more tailored channels for the diffusion of substrates and products, thereby leading to increased activities. Secondly, it is suggested that the different crystallinity of the COFs may contribute to the contrast catalytic performances. After catalysis, **Ir-4-*i*Pr** remained highly crystalline, as confirmed by the slight drop of surface area to 972 m²/g (Table S8). On the other hand, with the surface areas being only 26 and 68 m²/g, respectively, **Ir-4-H/Et** exhibited obviously decreased crystallinity compared to the pristine samples (Figure S6). Control experiments showed that amorphous **Ir-4-*i*Pr/Et** indeed afforded much lower yields than the crystalline counterparts in catalyzing the borylation reactions (Table 2, entries 1, 2, 5 and 6). It is not surprising that the solids with low or no crystallinity interrupt the uniform distribution of the Ir-bipy units and provide a decreased number of accessible active sites for the reactants, thus showing less effectiveness for the transformations.

Significantly, **Ir-4-*i*Pr** is much more active than the homogeneous counterpart in borylation of arenes. For example, at 100 °C, 0.4 mol% Ir(bipy)(COD)(OMe) (Ir-bipy) afforded 61% yield of the product in the borylation of benzene after 48 h (Table 2, entry 4) and then no further conversion of arene was detected with prolonged heating time. The higher activity of **Ir-4-*i*Pr** is likely due to active site isolation which prevents any intermolecular deactivation pathways. Moreover, **Ir-4-*i*Pr** displayed catalytic activities and regioselectivities that are comparable to or surpass those reported Ir(bpy)-based heterogeneous catalysts (Table S5).³⁰ The catalyst **Ir-4-*i*Pr** can be reused at least ten times in the borylation of 3-(trifluoromethyl)anisole without loss of catalytic activity (96-100% yield, Table S7). No further conversion of arene was detected after removal of the solid catalyst from the reaction mixture. ICP-OES analysis of the filtrate after the reaction revealed almost no leaching of Ir ions (~0.0016%). After ten cycles, the recovered catalysts remained high crystallinity and porosity (BET = 750 m²·g⁻¹, Figure 2h).

CONCLUSION

We have designed and synthesized a series of two-, three- and four-component 2D COFs decorated with sterically hydrophobic groups by imine condensation of triamine and di- or trialdehyde building blocks. Modulating the interlayer steric hindrance through controlling concentrations of alkyl groups, which can be readily tuned by using a MTV approach, allows access to 2D COFs with AA, AB or ABC stacking and moderate to high chemical stability. **Ir-4-*i*Pr** exhibits much higher catalytic activity than **Ir-4-Et/H** in C-H borylation of arenes because of the increased porosity and chemical stability. Further studies on the mechanism that how and why steric hindrances can guide the COFs sheets lock into a position during crystal growth to generate a certain stacking mode and deep insight into stacking mode transformation are greatly needed. This work provides a simple

approach to control layer stacking and chemical stability for 2D COFs, holding great promise for efficiently preparing a wide range of novel 2D COFs that will display interesting electronic, optic and catalytic properties.

ASSOCIATED CONTENT

Experimental procedures and characterization data. This material is available free of charge via the Internet at <http://pubs.acs.org>.

AUTHOR INFORMATION

Corresponding Author

*yongcui@sjtu.edu.cn

*liuy@sjtu.edu.cn

Notes

The authors declare no competing financial interest.

ACKNOWLEDGMENT

This work was financially supported by the National Science Foundation of China (Grants 21431004, 21522104 and 21620102001), the National Key Basic Research Program of China (Grant 2016YFA0203400), Key Project of Basic Research of Shanghai (17JC1403100 and 18JC1413200), and the Shanghai “Eastern Scholar” Program.

REFERENCES

- (a) Côté, A. P.; Benin, A. I.; Ockwig, N. W.; O’Keeffe, M.; Matzger, A. J.; Yaghi, O. M. *Science* **2005**, *310*, 1166. (b) Kandambeth, S.; Mallick, A.; Lukose, B.; Mane, M. V.; Heine, T.; Banerjee, R. *J. Am. Chem. Soc.* **2012**, *134*, 19524. (c) Bunck, D. N.; Dichtel, W. R. *J. Am. Chem. Soc.* **2013**, *135*, 14952. (d) Jin, E.; Asada, M.; Xu, Q.; Dalapati, S.; Addicoat, M. A.; Brady, M. A.; Xu, H.; Nakamura, T.; Heine, T.; Chen, Q.; Jiang, D. *Science* **2017**, *357*, 673. (e) Ma, T.; Kapustin, E. A.; Yin, S. X.; Liang, L.; Zhou, Z.; Niu, J.; Li, L.-H.; Wang, Y.; Su, J.; Li, J.; Wang, X.; Wang, W. D.; Wang, W.; Sun, J.; Yaghi, O. M. *Science* **2018**, *361*, 48.
- (a) Furukawa, H.; Yaghi, O. M. *J. Am. Chem. Soc.* **2009**, *131*, 8875. (b) Yang, Y.; Faheem, M.; Wang, L.; Meng, Q.; Sha, H.; Yang, N.; Yuan, Y.; Zhu, G. *ACS. Cent. Sci.* **2018**, *4*, 748. (c) Tilford, R. W.; Mugavero III, S. J.; Pellechia, P. J.; Lavigne, J. J. *Adv. Mater* **2008**, *20*, 2741.
- (a) Kang, Z.; Peng, Y.; Qian, Y.; Yuan, D.; Addicoat, M. A.; Heine, T.; Hu, Z.; Tee, L.; Guo, Z.; Zhao, D. *Chem. Mater.* **2016**, *28*, 1277. (b) Qian, H.-L.; Yang, C.-X.; Yan, X.-P. *Nat. Commun.* **2016**, *7*, 12104. (c) Oh, H.; Kalidindi, S. B.; Um, Y.; Bureekaew, S.; Schmid, R.; Fischer, R. A.; Hirscher, M. *Angew. Chem. Int. Ed.* **2013**, *52*, 13219. (d) Baldwin, L. A.; Crowe, J. W.; Pyles, D. A.; McGrier, P. L. *J. Am. Chem. Soc.* **2016**, *138*, 15134. (e) Dey, K.; Pal, M.; Rout, K. C.; Kunjattu, H. S.; Das, A.; Mukherjee, R.; Kharul, U. K.; Banerjee, R. *J. Am. Chem. Soc.* **2017**, *139*, 13083. (f) Han, X.; Huang, J.; Yuan, C.; Liu, Y.; Cui, Y. *J. Am. Chem. Soc.* **2018**, *140*, 892.
- (a) Li, H.; Pan, Q.; Ma, Y.; Guan, X.; Xue, M.; Fang, Q.; Yan, Y.; Valtchev, V.; Qiu, S. *J. Am. Chem. Soc.* **2016**, *138*, 14783. (b) Lin, S.; Diercks, C. S.; Zhang, Y. B.; Kornienko, N.; Nichols, E. M.; Zhao, Y. B.; Paris, A. R.; Kim, D.; Yang, P.; Yaghi, O. M.; Chang, C. J. *Science* **2015**, *349*, 1208. (c) Sun, Q.; Aguila, B.; Perman, J.; Nguyen, N.; Ma, S. *J. Am. Chem. Soc.* **2016**, *138*, 15790. (d) Lu, S.; Hu, Y.; Wan, S.; McCaffrey, R.; Jin, Y.; Gu, H.; Zhang, W. *J. Am. Chem. Soc.* **2017**, *139*, 17082.
- (a) Lin, G.; Ding, H.; Yuan, D.; Wang, B.; Wang, C. *J. Am. Chem. Soc.* **2016**, *138*, 3302. (b) Rao, M. R.; Fang, Y.; De Feyter,

- S.; Perepichka, D. F. *J. Am. Chem. Soc.* **2017**, *139*, 2421. (c) Peng, Y.; Huang, Y.; Zhu, Y.; Chen, B.; Wang, L.; Lai, Z.; Zhang, Z.; Zhao, M.; Tan, C.; Yang, N.; Shao, F.; Han, Y.; Zhang, H. *J. Am. Chem. Soc.* **2017**, *139*, 8698.
- (a) Wang, S.; Wang, Q.; Shao, P.; Han, Y.; Gao, X.; Ma, L.; Yuan, S.; Ma, X.; Zhou, J.; Feng, X.; Wang, B. *J. Am. Chem. Soc.* **2017**, *139*, 4258. (b) DeBlase, C. R.; Silberstein, K. E.; Truong, T.-T.; Abruña, H. D.; Dichtel, W. R. *J. Am. Chem. Soc.* **2013**, *135*, 16821. (c) Chandra, S.; Kundu, T.; Kandambeth, S.; BabaRao, R.; Marathe, Y.; Kunjir, S. M.; Banerjee, R. *J. Am. Chem. Soc.* **2014**, *136*, 6570. (d) Xu, Q.; Tao, S.; Jiang, Q.; Jiang, D. *J. Am. Chem. Soc.* **2018**, *140*, 7429. (e) Duhović, S.; Dincă, M. *Chem. Mater.* **2015**, *27*, 5487.
- (a) Fan, Y.; Wen, Q.; Zhan, T.-G.; Qi, Q.-Y.; Xu, J.-Q.; Zhao, X. *Chem. Eur. J.* **2017**, *23*, 5668. (b) Haase, F.; Gottschling, K.; Stegbauer, L.; Germann, L. S.; Gutzler, R.; Duppel, V.; Vyas, V. S.; Kern, K.; Dinnebier, R. E.; Lotsch, B. V. *Mater. Chem. Front.* **2017**, *1*, 1354.
- Ascherl, L.; Sick, T.; Margraf, J. T.; Lapidus, S. H.; Calik, M.; Hettstedt, C.; Karaghiosoff, K.; Döblinger, M.; Clark, T.; Chapman, K. W.; Auras, F.; Bein, T. *Nat. Chem.* **2016**, *8*, 310.
- Chen, X.; Addicoat, M.; Irle, S.; Nagai, A.; Jiang, D. *J. Am. Chem. Soc.* **2013**, *135*, 546.
- (a) Qian, C.; Xu, S. Q.; Jiang, G. F.; Zhan, T. G.; Zhao, X. *Chem. Eur. J.* **2016**, *22*, 17784. (b) Wang, X. R.; Han, X.; Zhang, J.; Wu, X. W.; Liu, Y.; Cui, Y. *J. Am. Chem. Soc.* **2016**, *138*, 12332. (c) Ma, H.-C.; Kan, J.-L.; Chen, G.-J.; Chen, C.-X.; Dong, Y.-B. *Chem. Mater.* **2017**, *29*, 6518. (d) Zhu, M. W.; Xu, S. Q.; Wang, X. Z.; Chen, Y.; Dai, L.; Zhao, X. *Chem. Commun.* **2018**, *54*, 2308.
- (a) Wu, S.; Li, M.; Phan, H.; Wang, D.; Heng, T. S.; Ding, J.; Lu, Z.; Wu, J. *Angew. Chem. Int. Ed.* **2018**, *57*, 8007. (b) Das, G.; Biswal, B. P.; Kandambeth, S.; Venkatesh, V.; Kaur, G.; Addicoat, M.; Heine, T.; Verma, S.; Banerjee, R. *Chem. Sci.* **2015**, *6*, 3931. (c) Zhang, J.; Han, X.; Wu, X.; Liu, Y.; Cui, Y. *J. Am. Chem. Soc.* **2017**, *139*, 8277. (d) Stewart, D.; Antypov, D.; Dyer, M. S.; Pitcher, M. J.; Katsoulidis, A. P.; Chater, P. A.; Blanc, F.; Rosseinsky, M. J. *Nat. Commun.* **2017**, *8*, 1102. (e) Mullangi, D.; Shalini, S.; Nandi, S.; Choksi, B.; Vaidhyanathan, R. *J. Mater. Chem. A* **2017**, *5*, 8376.
- Lohse, M. S.; Bein, T. *Adv. Funct. Mater.* **2018**, *28*, 1870229.
- Xu, H.; Gao, J.; Jiang, D. *Nat. Chem.* **2015**, *7*, 905.
- Waller, P. J.; Lyle, S. J.; Osborn Popp, T. M.; Diercks, C. S.; Reimer, J. A.; Yaghi, O. M. *J. Am. Chem. Soc.* **2016**, *138*, 15519.
- Zhang, B.; Wei, M.; Mao, H.; Pei, X.; Alshimiri, S. A.; Reimer, J. A.; Yaghi, O. M. *J. Am. Chem. Soc.* **2018**, *140*, 9099.
- (a) Wei, P.; Qi, M.; Wang, Z.; Ding, S.; Yu, W.; Liu, Q.; Wang, L.; Wang, H.; An, W.; Wang, W. *J. Am. Chem. Soc.* **2018**, *140*, 4623. (b) Haase, F.; Troschke, E.; Savasci, G.; Banerjee, T.; Duppel, V.; Dörfler, S.; Grunde, M. M. J.; Burrow, A. M.; Ochsenfeld, C.; Kaskel, S.; Lotsch, B. V. *Nat. Commun.* **2018**, *9*, 2600.
- Li, X.; Zhang, C.; Cai, S.; Lei, X.; Altoe, V.; Hong, F.; Urban, J. J.; Ciston, J.; Chan, E. M.; Liu, Y. *Nat. Commun.* **2018**, *9*, 2998.
- Han, X.; Xia, Q.; Huang, J.; Liu, Y.; Tan, C.; Cui, Y. *J. Am. Chem. Soc.* **2017**, *139*, 8693.
- The MTV approach has been explored to expand structural complexity, improve chemical stability and advance optic and electronic properties of COFs. (a) Huang, N.; Zhai, L.; Coupry, D. E.; Addicoat, M. A.; Okushita, K.; Nishimura, K.; Heine, T.; Jiang, D. *Nat. Commun.* **2016**, *7*, 12325. (b) Li, X.; Gao, Q.; Wang, J.; Chen, Y.; Chen, Z. H.; Xu, H. S.; Tang, W.; Leng, K.; Ning, G. H.; Wu, J.; Xu, Q. H.; Quek, S. Y.; Lu, Y.; Loh, K. P. *Nat. Commun.* **2018**, *9*, 2335. (c) Pang, Z.-F.; Xu, S.-Q.; Zhou, T.-

- 1 Y.; Liang, R.-R.; Zhan, T.-G.; Zhao, X. *J. Am. Chem. Soc.* **2016**,
2 138, 4710.
- 3 20. (a) Matsumoto, M.; Dasari, R. R.; Ji, W.; Feriante, C. H.;
4 Parker, T. C.; Marder, S. R.; Dichtel, W. R. *J. Am. Chem. Soc.*
5 **2017**, 139, 4999. (b) Li, Z. J.; Ding, S. Y.; Xue, H. D.; Cao, W.;
6 Wang, W. *Chem. Commun.* **2016**, 52, 7217. (c) Zhai, L.; Huang,
7 N.; Xu, H.; Chen, Q.; Jiang, D. *Chem. Commun.* **2017**, 53, 4242.
8 (d) Dong, J.; Wang, Y.; Liu, G.; Cheng, Y.; Zhao, D.
9 *CrystEngComm.* **2017**, 19, 4899.
- 10 21. Kaleeswaran, D.; Vishnoi, P.; Murugavel, R. *J. Mater. Chem.*
11 *C.* **2015**, 3, 7159.
- 12 22. (a) Cavka, J. H.; Jakobsen, S.; Olsbye, U.; Guillou, N.;
13 Lamberti, C.; Bordiga, S.; Lillerud, K. P. *J. Am. Chem. Soc.* **2008**,
14 130, 13850. (b) Férey, G.; Mellot-Draznieks, C.; Serre, C.;
15 Millange, F.; Dutour, J.; Surblé, S.; Margiolaki, I. *Science.* **2005**,
16 309, 2040. (c) Park, K. S.; Ni, Z.; Cote, A. P.; Choi, J. Y.; Huang,
17 R.; Uribe-Romo, F. J.; Chae, H. K.; O'Keeffe, M.; Yaghi, O. M.
18 *Proc. Natl. Acad. Sci. U S A* **2006**, 103, 10186. (d) Wang, K.; Lv,
19 X. L.; Feng, D.; Li, J.; Chen, S.; Sun, J.; Song, L.; Xie, Y.; Li, J.
20 R.; Zhou, H. C. *J. Am. Chem. Soc.* **2016**, 138, 914.
- 21 23. Tao, Y.; Kanoh, H.; Abrams, L.; Kaneko, K. *Chem. Rev.* **2006**,
22 106, 896.
- 23 24. Zhao, D.; Huo, Q.; Feng, J.; Chmelka, B. F.; Stucky, G. D. *J.*
24 *Am. Chem. Soc.* **1998**, 120, 6024.
- 25 25. Pang, Z. F.; Zhou, T. Y.; Liang, R. R.; Qi, Q. Y.; Zhao, X.
26 *Chem. Sci.* **2017**, 8, 3866.
- 27 26. Kaes, C.; Katz, A.; Hosseini, M. W. *Chem. Rev.* **2000**, 100,
28 3553.
- 29 27. Mkhaliid, I. A. I.; Barnard, J. H.; Marder, T. B.; Murphy, J. M.;
30 Hartwig, J. F. *Chem. Rev.* **2010**, 110, 890.
- 31 28. (a) Waki, M.; Maegawa, Y.; Hara, K.; Goto, Y.; Shirai, S.;
32 Yamada, Y.; Mizoshita, N.; Tani, T.; Chun, W. J.; Muratsugu, S.;
33 Tada, M.; Fukuoka, A.; Inagaki, S. *J. Am. Chem. Soc.* **2014**, 136,
34 4003. (b) Wu, F. S.; Feng, Y.; Jones, C. W. *Acc. Catal.* **2014**, 4,
35 1365.
- 36 29. Manna, K.; Zhang, T.; Greene, F. X.; Lin, W. *J. Am. Chem.*
37 *Soc.* **2015**, 137, 2665.
- 38 30. (a) Santoro, S.; Kozhushkov, S. I.; Ackermann, L.; Vaccaro,
39 L. *Green. Chem.* **2016**, 18, 3471. (b) Iwai, T.; Harada, T.; Hara,
40 K.; Sawamura, M. *Angew. Chem. Int. Ed.* **2013**, 52, 12322.
- 41
42
43
44
45
46
47
48
49
50
51
52
53
54
55
56
57
58
59
60

Topic of Content

